arXiv:cond-mat/9703077v1 [cond-mat.mtrl-sci] 7 Mar 1997

X-ray absorption and resonant inelastic x-ray scattering in the rare earths

Michel van Veenendaal and Robert Benoist
European Synchrotron Radiation Facility, B.P. 220, F-38043 Grenoble Cédex, France.

(February 1, 2008)

This paper makes a comparison between x-ray absorption (XAS) and resonant inelastic x-ray scattering (RIXS) in the rare earths. Atomic calculations are given for $2p \rightarrow 4f$ and $2p \rightarrow 5d$ XAS. The latter calculation includes the contraction and expansion of the $5d$ orbitals resulting from the complete exchange interaction with the $4f$ electrons. The radiative decay of the XAS final states is described for the situations where the core hole created in the absorption process is filled by a valence electron or by an electron from a shallower core level. RIXS spectra, $4f^n \rightarrow \underline{3d}4f^{n+1} \rightarrow 4f^n$, integrated over the outgoing photon energy (fluorescence yield) are compared with $3d \rightarrow 4f$ XAS. Sum rules related to XAS and RIXS and their applicability are discussed.

PACS numbers: 61.10.Dp, 78.70.Ck, 78.70.Dm, 78.70.En

I. INTRODUCTION

Experiments on rare earth systems have made an important contribution to the development of magnetic x-ray dichroism and resonant magnetic scattering. Both circular[1] and linear[2] magnetic x-ray dichroism have been observed for the first time in rare earths. The first satisfactory explanation of resonant magnetic scattering was done for Holmium metal.[3,4] The electronic structure of rare earths is determined by the interaction between electrons in the localized $4f$ orbitals and in the broad $5d$ band. Spectroscopies involving the $4f$ shell can usually be successfully described by atomic multiplet theory. But whereas, e.g., magnetic x-ray dichroism at the M_{45} edges is rather well understood, the L_{23} spectra, dominated by the dipolar $2p \rightarrow 5d$ transitions, pose more problems. In the interpretation one has to take into account two effects.

First, one observes pre-edge features[5,6] that are weak in the isotropic spectra but have a strong circular dichroic signal. That these structures arise from quadrupolar transitions into the $4f$ shell has been established by resonant elastic $\sigma \rightarrow \pi$ x-ray scattering,[3,4] by the observation of a non-dipolar angular dependence of the circular dichroic XAS,[7,8] by resonant Raman spectroscopy,[9,10] and by partial deconvolution of the life time broadening.[11]

Second, the finite integrated intensity of the circular dichroism of the $2p \rightarrow 5d$ transitions results, not only from the polarization of the $5d$ electrons in the ground state, but also from a dependence of the $2p$-$5d$ radial matrix elements on the direction of the $5d$ moment relative to that of the $4f$.[7,12] Therefore, band effects[7] and the full df-Coulomb interaction[13,14] have to be included in the interpretation of the spectral line shape and the variations in the L_{23} circular dichroic branching ratios.

A complication in the interpretation of RIXS is that the deexcitation cannot be simply decoupled from the absorption step as can be done when the excitation is far above threshold. Furthermore, the decay is different for transitions between two core levels or between the valence shell and a core level.

For systems where a detailed description of the spectral line shape is complex, useful results can still be obtained from statistical methods. For XAS and x-ray scattering sum rules exist that relate the integrated intensities to ground state properties.[15–18] These sum rules rely on a number of approximations. In general a constant radial matrix element is required. For sum rules that consider the spin-orbit manifolds separately one has to assume that the edges can be distinguished by the j-value of the core hole. For fluorescence yield no exact sum rules have been derived so far and the application of XAS sum rules requires numerical validation.[19] In this paper we address the applicability of the sum rules.

The paper is divided as follows. First, we show the separation of the geometric and electronic part for XAS and RIXS. Section III gives a derivation for the angular distributions for some common experimental situations. Section IV is devoted to the spectral functions and their sum rules. We describe the spectral line shape of the XAS spectra at the L_{23} edge. For the dipolar part we include the effects of contraction and expansion of the $5d$ orbital by the df-Coulomb interaction. RIXS results are discussed for spectroscopies involving the $4f$ shell. A comparison is made between the radiative decay in spectroscopies where the intermediate state core hole is filled by a valence electron or by an electron from a shallower core level. We end with the conclusions.

II. INTENSITIES

The intershell transitions as a result of the absorption or emission of a x-ray photon are described by $H_{\rm int} = \frac{e}{2m}\{\mathbf{p}\cdot\mathbf{A} + \mathbf{A}\cdot\mathbf{p}\}$. Expanding the vector potential in plane waves gives

$$\mathbf{A} = \sum_{\mathbf{k}\boldsymbol{\epsilon}} \sqrt{\frac{\hbar}{2\omega\epsilon_0\Omega}} \left\{\boldsymbol{\epsilon} a_{\mathbf{k}\boldsymbol{\epsilon}} e^{i\mathbf{kr}} + \text{h.c.}\right\}, \tag{1}$$

where Ω is a normalization volume and $a_{\mathbf{k}\boldsymbol{\epsilon}}$ annihilates a photon with momentum $\mathbf{k}$ and polarization vector ϵ.

The absorption intensity is then given by Fermi's golden rule:

$$I(\hat{\mathbf{k}}\boldsymbol{\epsilon}\omega) = \frac{2\pi}{\hbar}\sum_n |\langle n|H_{\text{int}}|g\rangle|^2 \delta(\omega + E_g - E_n)\rho_\omega, \qquad (2)$$

with the density of oscillators given by $\rho_\omega = \frac{\Omega}{8\pi^3}\frac{\omega^2}{\hbar c^3}$. The different multipoles of the spectrum are obtained by expanding the plane wave in Bessel functions and spherical harmonics, i.e,

$$\mathrm{e}^{i\mathbf{kr}} = \sum_t [t] i^t j_t(kr) \hat{\mathbf{k}}^{(t)} \cdot \hat{\mathbf{r}}^{(t)}, \qquad (3)$$

with $[a \ldots b] = (2a+1)\ldots(2b+1)$. We use here the shorthands $\mathbf{k}^{(l)} = k^l \mathbf{C}^l(\hat{\mathbf{k}})$ and for spherical tensors of rank one: $\mathbf{k} = \mathbf{k}^{(1)}$. Note that $\hat{k} = 1$. For $kr \ll 1$ one has $j_t(kr) \cong (kr)^t/[t]!!$. With the use of the orthogonality relation one then obtains

$$\mathbf{p}\cdot\boldsymbol{\epsilon}\mathrm{e}^{i\mathbf{kr}} = \sum_{tQ} [tQ] \frac{i^t}{[t]!!} [\mathbf{p}, \mathbf{r}^{(t)}]^Q \cdot [\boldsymbol{\epsilon}, \mathbf{k}^{(t)}]^Q, \qquad (4)$$

where the tensor couplings are defined in the Appendix. It is convenient to define the operators

$$\mathbf{V}^{tQ} = \frac{b_{tQ}(k)}{2im\omega}\{\ [\mathbf{p}, \mathbf{r}^{(t)}]^Q + (-1)^Q [\mathbf{r}^{(t)}, \mathbf{p}]^Q\ \}, \qquad (5)$$

where the factors $b_{tQ}(k)$ will be chosen in such a way that nicely defined operators are obtained, see Table I. For $tQ = 01$ (electric dipole) and $b_{01}(k) = \sqrt{3}$ we have

$$\langle n|\mathbf{V}^{01}|g\rangle = \frac{b_{01}(k)}{\sqrt{3}im\omega}\langle n|\mathbf{p}|g\rangle = \frac{1}{\hbar\omega}\langle n|[\frac{p^2}{2m}, \mathbf{r}]|g\rangle \cong \langle n|\mathbf{r}|g\rangle.$$

By using the definition for the outer product and $b_{11}(k) = \sqrt{\frac{3}{2}}k$, we find that $\mathbf{V}^{11}$ is equal to $\frac{b_{11}(k)}{im\omega}[\mathbf{p}, \mathbf{r}]^1 = \frac{\alpha}{2}\frac{a_0}{\hbar}\mathbf{L}$, with α the fine-structure constant and a_0 the Bohr radius. $\mathbf{V}^{11}$ forms together with the $g_S\mathbf{S}$ term the magnetic dipole operator. Magnetic dipole transitions are about $(\alpha/2)^2$, i.e., five orders of magnitude smaller than electric dipole transitions of the same wavelength. Furthermore, we have for the electric quadrupole operator, $\mathbf{V}^{12} = \mathbf{r}^{(2)}$, that $b_{12}(k) = \sqrt{30}$.

TABLE I. Relevant constants for electric dipole (tQ=01), magnetic dipole (11), and electric quadrupole (12) transitions. The factors $b_{tQ}(k)$ appear in the definition of the operators $\mathbf{V}^{tQ}$. The B_Q^2 give the relative probabilities of dipolar and quadrupolar transitions. The factors D_{tQ} are used in the definition of the angular dependence $\mathbf{T}^{tQz}$.

	t	Q	$\mathbf{V}^{tQ}$	$b_{tQ}(k)$	B_Q^2	D_{tQ}
el. dip.	0	1	$\mathbf{r}$	$\sqrt{3}$	$\frac{1}{3}$	3
magn. dip.	1	1	$\frac{\alpha}{2}\frac{a_0}{\hbar}\mathbf{L}$	$\sqrt{\frac{3}{2}}k$	$\frac{1}{3}$	$3\sqrt{2}$
el. quad.	1	2	$\mathbf{r}^{(2)}$	$-\sqrt{30}$	$\frac{1}{15}(\frac{k}{2})^2$	$-5\sqrt{2}$

The multipole expansion enables us to separate the absorption intensity into a geometric and an electronic part, i.e.,

$$\begin{aligned} I(\hat{\mathbf{k}}\boldsymbol{\epsilon}\omega) &= \frac{2\pi}{\hbar}N_\omega \sum_{tQn} B_Q^2 D_{tQ}^2\ |\langle n|[\boldsymbol{\epsilon}, \mathbf{k}^{(t)}]^Q \cdot \mathbf{V}^{tQ}|g\rangle|^2 \\ &\qquad \times\delta(\omega + E_g - E_n) \\ &= \frac{2\pi}{\hbar}N_\omega \sum_{tQz} B_Q^2\ \mathbf{T}^{tQz}(\hat{\mathbf{k}}\boldsymbol{\epsilon}) \cdot \mathbf{I}^{tQz}(\omega), \end{aligned} \qquad (6)$$

where cross terms between different tQ values have been omitted. The following factors have been defined: $N_\omega = \frac{e^2\omega^3}{16\pi^3\epsilon_0 c^3}$; $B_Q = (\frac{k}{2})^{Q-1}([Q]!!)^{-\frac{1}{2}}$ gives the relative transition probability, where for the dipolar and quadrupolar contributions one has $B_2^2/B_1^2 = \frac{1}{5}(\frac{k}{2})^2$; and $D_{tQ} = [tQ]k^t/([t]!!b_{tQ}(k)B_Q)$. The different multipole spectra are given by

$$\mathbf{I}^{tQz}(\omega) = \frac{\Gamma}{\pi}\sum_n \frac{1}{|\mathcal{E}_n|^2}\mathbf{I}^{tQz}(gnng) \qquad (7)$$

with $\mathcal{E}_n = \omega + E_g - E_n + i\frac{\Gamma}{2}$ where Γ is the lifetime broadening of the XAS final states; the different combinations of the matrix elements are defined as

$$\mathbf{I}^{tQz}(abcd) = [\langle a|(\mathbf{V}^\dagger)^{tQ}|b\rangle, \langle c|\mathbf{V}^{tQ}|d\rangle]^z n_{Qz}^{-1}\ , \qquad (8)$$

where the normalization constants n_{Qz} are defined in the Appendix. The angular distribution is given by

$$\mathbf{T}^{tQz}(\hat{\mathbf{k}}\boldsymbol{\epsilon}) = [z] D_{tQ}^2 [[\boldsymbol{\epsilon}^*, \hat{\mathbf{k}}^{(t)}]^Q, [\boldsymbol{\epsilon}, \hat{\mathbf{k}}^{(t)}]^Q]^z n_{Qz}\ . \qquad (9)$$

The RIXS intensity is proportional to

$$\begin{aligned} I(\hat{\mathbf{k}}\boldsymbol{\epsilon}\omega, \hat{\mathbf{k}}'\boldsymbol{\epsilon}'\omega') = &\frac{2\pi}{\hbar}\sum_f \left|\sum_n \frac{\langle f|H_{\text{int}}|n\rangle\langle n|H_{\text{int}}|g\rangle}{\omega + E_g - E_n + i\frac{\Gamma}{2}}\right|^2 \\ &\times\delta(\omega + E_g - \omega' - E_f)\rho_{\omega'}\rho_\omega. \end{aligned} \qquad (10)$$

In the remainder of the paper we consider the different multipole transitions separately; to reduce the number of indices we remove the tQ of the transitions. In a way similar to that for XAS we find for the RIXS cross section with Q-polar excitation followed by a Q'-polar deexcitation

$$\begin{aligned} I(\hat{\mathbf{k}}\boldsymbol{\epsilon}\omega, \hat{\mathbf{k}}'\boldsymbol{\epsilon}'\omega') = &\frac{2\pi}{\hbar}N_{\omega'}B_{Q'}^2 N_\omega B_Q^2 \\ &\times \sum_{zz'r} \mathbf{T}^{zz'r}(\hat{\mathbf{k}}\boldsymbol{\epsilon}, \hat{\mathbf{k}}'\boldsymbol{\epsilon}') \cdot \mathbf{I}^{zz'r}(\omega, \omega'). \end{aligned} \qquad (11)$$

The electronic part has now become a tensor product of absorption and emission

$$\begin{aligned} \mathbf{I}^{zz'r}(\omega, \omega') = &[r]\frac{\gamma}{\pi}\sum_{nn'f}\frac{1}{|\mathcal{E}_f|^2}\frac{1}{\mathcal{E}_{n'}^*\mathcal{E}_n} \\ &\times [\mathbf{I}^{z'}(n'ffn), \mathbf{I}^z(gn'ng)]^r n_{zz'r}\ , \end{aligned} \qquad (12)$$

where $\mathcal{E}_f = \omega + E_g - \omega' - E_f + i\frac{\gamma}{2}$ with γ the lifetime broadening of the x-ray inelastic scattering final states. The angular dependence is given by

$$\mathbf{T}^{zz'r}(\hat{\mathbf{k}}\boldsymbol{\epsilon}, \hat{\mathbf{k}}'\boldsymbol{\epsilon}') = [\mathbf{T}^{z'}(\hat{\mathbf{k}}'\boldsymbol{\epsilon}'), \mathbf{T}^z(\hat{\mathbf{k}}\boldsymbol{\epsilon})]^r n_{zz'r}^{-1}\ . \qquad (13)$$

III. ANGULAR DEPENDENCE

The tensors for the angular dependence are chosen in such a way that $\mathbf{T}^0=1$ for $tQ=01,11,12$. For electric dipole transitions $\mathbf{T}^z$ is $\hat{\mathbf{k}}$ independent, and the $\zeta=0$ component is, with respect to the $\hat{\mathbf{Z}}$-axis of our system,

$$T_0^z(\boldsymbol{\epsilon}) = 3[z](-1)^{1+z} n_{Qz} n_{11z} U^{11z}(\boldsymbol{\epsilon}^*, \boldsymbol{\epsilon}, \hat{\mathbf{Z}}), \tag{14}$$

where the bipolar spherical harmonics[20] are given by $U^{xyz}(\mathbf{a},\mathbf{b},\mathbf{c}) = (-)^{y+z}\underline{n}_{xyz}^{-1}[\mathbf{a}^{(x)}\mathbf{b}^{(y)}]^z \cdot \mathbf{c}^{(z)}$. The bipolar spherical harmonics with xyz relevant for dipolar transitions are given in Table II; expressions for higher values of xyz are given by Thole and Van der Laan.[21] For general multipole transitions it is more convenient to recouple the angular dependence

$$\mathbf{T}^z(\hat{\mathbf{k}}\boldsymbol{\epsilon}) = (-1)^{1+t+z} D_{tQ}^2 \sum_{xy} [xyz] \left\{ \begin{array}{ccc} 1 & x & 1 \\ t & y & t \\ Q & z & Q \end{array} \right\} \times [[\boldsymbol{\epsilon}^*, \boldsymbol{\epsilon}]^x, [\hat{\mathbf{k}}^{(t)}, \hat{\mathbf{k}}^{(t)}]^y]^z n_{Qz} \ . \tag{15}$$

It is straightforward to show that for left and right circularly polarized light one has

$$\frac{1}{2}([\boldsymbol{\epsilon}_+^*, \boldsymbol{\epsilon}_+]^x + (-1)^{x+m}[\boldsymbol{\epsilon}_-^*, \boldsymbol{\epsilon}_-]^x) = \left\{ \begin{array}{cc} a_x \underline{n}_{11x} C^x(\hat{\mathbf{k}}) & m=0 \\ 0 & m=1 \end{array} \right. ,$$

with $a_x = 1, \frac{2}{3}i, -\frac{1}{2}$ for $x=0,1,2$. After that one finds with the use of the theorem to couple two spherical harmonics of the same vector (see Appendix) that the angular dependence is a function of $\mathbf{C}^z(\hat{\mathbf{k}})$,[5]

$$\frac{1}{2}(\mathbf{T}^z(\hat{\mathbf{k}}\boldsymbol{\epsilon}_+) + (-1)^{z+m}\mathbf{T}^z(\hat{\mathbf{k}}\boldsymbol{\epsilon}_-)) = \left\{ \begin{array}{cc} \mathcal{T}_z \mathbf{C}^z(\hat{\mathbf{k}}) & m=0 \\ 0 & m=1 \end{array} \right. \tag{16}$$

where the coefficients

$$\mathcal{T}_z = (-)^{1+t+z} \sum_{xy} [xyz] a_x D_{tQ}^2 \left\{ \begin{array}{ccc} 1 & x & 1 \\ t & y & t \\ Q & z & Q \end{array} \right\} n_{Qz} \underline{n}_{11x} n_{tty} n_{xyz}$$

are given in Table III.

IV. SPECTRA AND SUM RULES

A. XAS into the $4f$ shell

Here we consider two absorption edges often studied: the L_{23}-edges, corresponding to transitions from the $2p$ orbital into the valence shell and the M_{45}-edges that are dominated by the dipolar $3d \rightarrow 4f$ transitions. The electric dipolar and quadrupolar transition operators are given by the Wigner-Eckart theorem:

$$\langle n|V_q|g\rangle = P_{cl} \sum_{\gamma\lambda\sigma} (-)^{l-\lambda} \left(\begin{array}{ccc} l & Q & c \\ -\lambda & q & \gamma \end{array} \right) \langle n| l_{\lambda\sigma}^\dagger c_{\gamma\sigma} |g\rangle,$$

where $l_{\lambda\sigma}^\dagger$ creates an electron in shell l with orbital component λ and spin σ. The reduced matrix element is given by

$$P_{cl}(Q) = (-1)^l n_{lQc} [lc]^{\frac{1}{2}} \int dr R_{n_l l}(r) r^Q R_{n_c c}(r). \tag{17}$$

For rare earths the crystal fields on the $4f$ electrons are often negligibly small and one can assume spherical symmetry (SO_3). For a magnetic system the symmetry is lowered to SO_2 and the J-values branch into $M_J = -J, \ldots, J$. Here we take the magnetic axis along the $\hat{\mathbf{Z}}$-axis and the ground state to be $M_J = J$. To obtain a non-zero intensity the total transition operator has to be totally symmetric. This means we have to consider $I_0^z(\omega)$ for XAS and $I_0^{zz'r}(\omega,\omega')$ for RIXS. I_0^z is a combination of the matrix elements $I_q(gnng) = \langle g|V_q^\dagger|n\rangle\langle n|V_q|g\rangle$. The combinations for $Q=1,2$ are given in Table IV. For dipolar transitions we have the well-known spectra: isotropic (I_0^0), circular dichroic (I_0^1), and linear dichroic (I_0^2).

Figures 1-4 give the XAS spectra for transitions into the $4f$-shell at the $L_{2,3}$ and $M_{4,5}$ edges. Calculations were done in the atomic limit using Cowan's programs.[22] The Hamiltonian includes the Coulomb interactions in the $4f$ shell and those between the $4f$ shell and the core hole and the spin-orbit coupling. Parameters were obtained in the Hartree-Fock limit and the values for the Coulomb interaction were scaled down to 80 % to account for screening effects. The zero of the energy scale corresponds to the energy of the lowest eigenstate in a spin-orbit manifold. Figure 1 gives the isotropic $2p \rightarrow 4f$ XAS spectrum. The used Lorentzian of 2 eV is smaller than the expected $2p$ lifetime broadening. This was done since recent experiments by Loeffen *et al.*[11] demonstrate the possibility of partial deconvolution of the lifetime broadening. By deconvoluting high-quality XAS data by a Lorentzian with a width of 3 eV, they obtained a clear separation of dipolar and quadrupolar features. Also the spectral line shape of the pre-edge structures was in agreement with multiplet calculations. This method seems to be well suited to

TABLE II. Bipolar spherical harmonic $U^{xyz}(\mathbf{a},\mathbf{b},\mathbf{c})$ relevant for the angular dependence of dipolar transitions.

$$U^{110} = \mathbf{a}\cdot\mathbf{b}$$
$$U^{111} = \tfrac{2}{3}(\mathbf{a}\times\mathbf{b})\cdot\mathbf{c}$$
$$U^{112} = \tfrac{3}{2}(\mathbf{a}\cdot\mathbf{c})(\mathbf{b}\cdot\mathbf{c}) - \tfrac{1}{2}(\mathbf{a}\cdot\mathbf{b})$$

TABLE III. Coeficients $\mathcal{T}_z$ defined in Eqn.(16) for Q=1,2 and $z=0,\ldots,2Q$.

$z=$	0	1	2	3	4
$Q=1$	1	$-\frac{3}{2}$	$\frac{1}{2}$		
2	1	-1	$-\frac{5}{7}$	1	$-\frac{2}{7}$

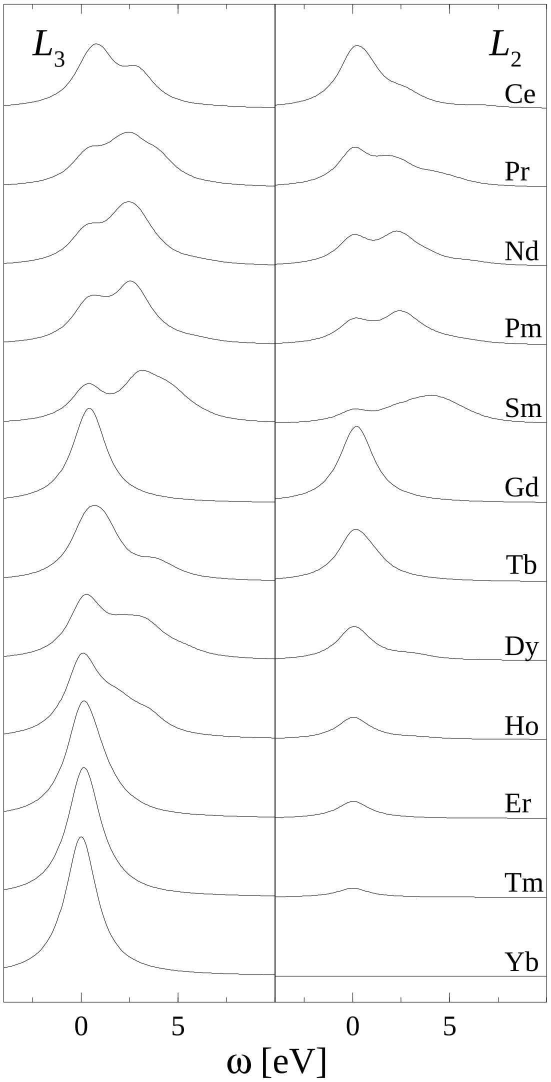

FIG. 1. Isotropic quadrupolar $2p \rightarrow 4f$ XAS spectra as a function of excitation energy ω for trivalent rare-earth ions. The left and right panel show the L_3 and L_2 edge, respectively. Spectra for the L_2 edge have been scaled by a factor two.

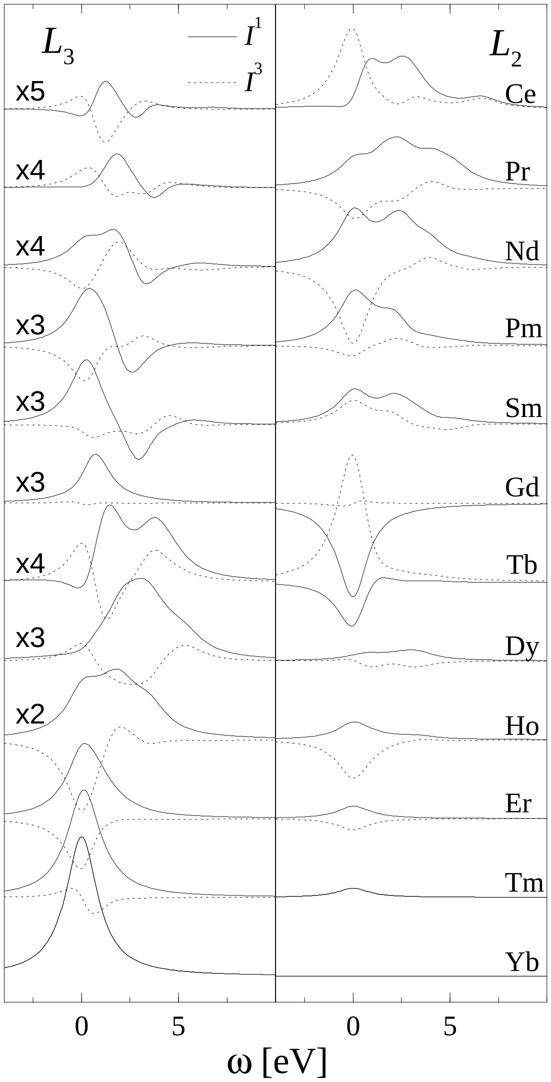

FIG. 2. Quadrupolar $2p \rightarrow 4f$ XAS spectra as a function of excitation energy ω for trivalent rare-earth ions. The spectrum for left minus right circularly polarized light is a angular dependent combination of I^1 (solid line) and I^3 (dotted line), see text. The left and right panel show the L_3 and L_2 edge, respectively. Spectra for the L_2 edge have been scaled by a factor two. Furthermore, some of the spectra are scaled relative to the spectra of Fig. 1. The scaling also applies to the right panel.

study the relative contributions of quadrupolar and dipolar transitions. The spectrum obtained after taking the difference between left and right circularly polarized light is a combination of I_0^z with odd z. Using Eqn. (16) we obtain[5]

$$\frac{1}{2}\{I(\hat{\mathbf{k}}\boldsymbol{\epsilon}^{+}\omega) - I(\hat{\mathbf{k}}\boldsymbol{\epsilon}^{-}\omega)\} = \frac{2\pi}{\hbar}N_\omega B_2^2\{-C_0^1(\hat{\mathbf{k}})I_0^1(\omega) + C_0^3(\hat{\mathbf{k}})I_0^3(\omega)\}, \tag{18}$$

where $C_0^z(\hat{\mathbf{k}})$ are Legendre polynomials of order z, i.e., $P^z(\cos\theta)$ with θ the angle between the direction of the light and the magnetic axis. The spectra $I_0^1(\omega)$ and $I_0^3(\omega)$ are given in Fig. 2.

TABLE IV. The spectra I_0^z expressed in I_q for Q=1,2.

Q=1 (dipolar)	$I_0^0 = I_1 + I_0 + I_{-1}$
	$I_0^1 = I_1 - I_{-1}$
	$I_0^2 = I_1 - 2I_0 + I_{-1}$
Q=2 (quadrupolar)	$I_0^0 = I_2 + I_1 + I_0 + I_{-1} + I_{-2}$
	$I_0^1 = I_2 + \frac{1}{2}I_1 - \frac{1}{2}I_{-1} - I_{-2}$
	$I_0^2 = I_2 - \frac{1}{2}I_1 - I_0 - \frac{1}{2}I_{-1} + I_{-2}$
	$I_0^3 = I_2 - 2I_1 + 2I_{-1} - I_{-2}$
	$I_0^4 = I_2 - 4I_1 + 6I_0 - 4I_{-1} + I_{-2}$

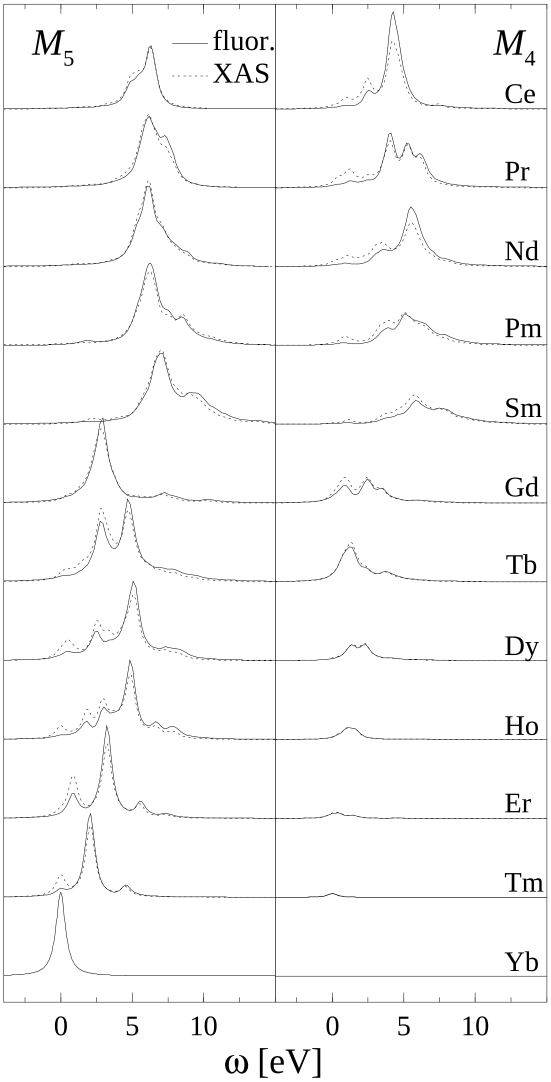

FIG. 3. Isotropic dipolar XAS spectra ($4f^n \rightarrow \underline{3d}4f^{n+1}$, dotted line) and fluorescence spectra for isotropic incoming and outgoing light ($4f^n \rightarrow \underline{3d}4f^{n+1} \rightarrow 4f^n$, solid line) as a function of excitation energy ω for trivalent rare-earth ions. XAS and fluorescence have been normalized to the intensity integrated over both edges; the scaling between spectra for different ions is arbitrary. The left and right panel show the M_5 and M_4 edge, respectively.

Figures 3 and 4 show, respectively, the isotropic and circular dichroic $M_{4,5}$ XAS spectra (Γ=0.8 eV). These spectra have been published earlier[23–25] and are included for comparison with the fluorescence yield spectra.

The behaviour of the intensities can be related to ground state expectation values by sum rules.[15,16,26] For $l = c + Q$ one can reduce the expressions to[27,28]

$$I_0^z(j) = \int_j d\omega I_0^z(\omega) = \frac{P_{cl}^2}{[cl]} \sum_{xy} M_y(j) N_{xyz} \langle w_0^{xyz} \rangle \qquad (19)$$

with $M_y(j)$=$c+1, c, c, -c$ for jy=j^+0, j^+1, j^-0, j^-1 ($j^\pm = l \pm s$) and N_{xyz}=$1, \frac{z}{[z]}, \frac{z+1}{[z]}$ for $xyz = z0z; z-1, 1, z; z+1, 1, z$. The coupled tensor operators are defined as[27,29]

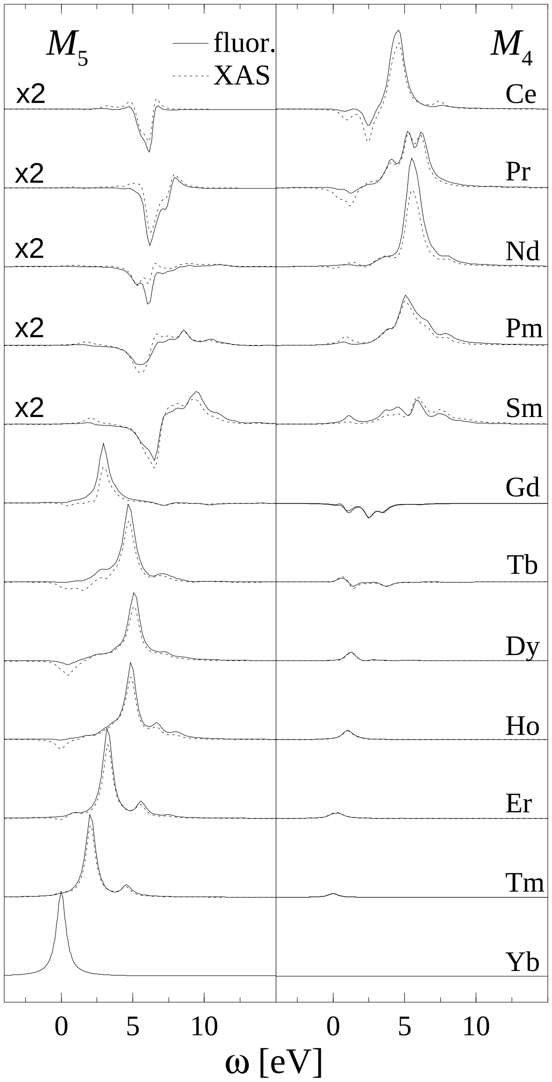

FIG. 4. Same as Fig. 3 but now for left minus right circularly polarized incoming light. Some of the spectra are scaled relative to the spectra of Fig. 3. The scaling applies also to the right panel.

$$w_\zeta^{xyz} = \sum_{\lambda\lambda'\sigma\sigma'\xi\eta} (-)^{l-\lambda'+s-\sigma} \begin{pmatrix} l & x & l \\ -\lambda' & \xi & \lambda \end{pmatrix} \begin{pmatrix} s & y & s \\ -\sigma' & \eta & \sigma \end{pmatrix}$$
$$\times (-)^{z-\zeta} \begin{pmatrix} x & y & z \\ -\xi & -\eta & \zeta \end{pmatrix} l_{\lambda'\sigma'} l_{\lambda\sigma}^\dagger \; n_{lx}^{-1} n_{sy}^{-1} \underline{n}_{xyz}^{-1} \qquad (20)$$

with s=$\frac{1}{2}$. The operators are spin independent and dependent for $y = 0$ and 1, respectively. These hole coupled tensor operators are related to the electron operators defined by Carra *et al.*[30] via O^{xyz}=$2[l]\delta_{x,0}\delta_{y,0} - (-1)^z r_{lx} r_{sy} w_0^{xyz}$ with $r_{lx} = \frac{(2l)!}{2^x(2l-x)!}$. The advantage of using normalized operators over Judd's operators[29] is

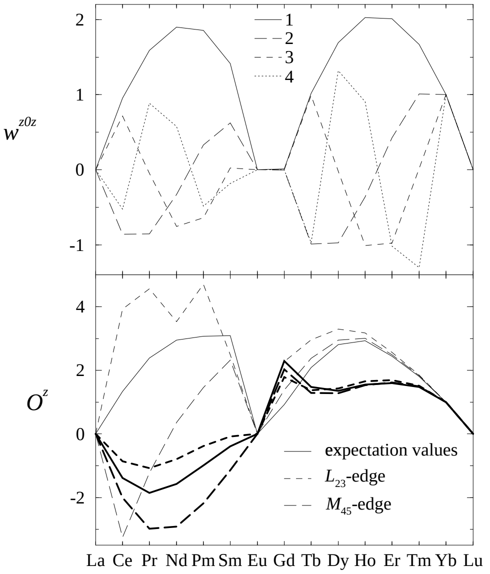

FIG. 5. The upper panel shows the ground state expectation values of w^{z0z} for trivalent rare-earth ions for z= 1 (solid line), 2 (long-dashed), 3 (dashed), and 4 (dotted). The lower panel shows the ground state expectation value of $O^z = \frac{z}{[z]} w^{z-1,1,0} + \frac{z+1}{[z]} w^{z+1,1,z}$ (solid line). The dashed and long-dashed lines show $n_h[I_0^z(j^+) - \frac{c+1}{c} I_0^z(j^-)]$ for the L_{23} and M_{45} edges, respectively. This quantity is equal to O^z according to the sum rules, see text. The thin and thick lines correspond to z=0 and 1, respectively.

that the square roots are removed from the expressions. They are normalized in such a way that the expectation values are unity for a ground state with one hole and $M_J = J = l + \frac{1}{2}$ (i.e., for rare earths the ground state of Yb^{3+}, $f^{13}(^2F_{\frac{7}{2}}; M_J = \frac{7}{2})$). Some typical examples are the number of holes: $n_h = w_0^{000}$, the orbital and spin magnetic moments: $L_z = l w_0^{101}$ and $S_z = s w_0^{011}$, respectively, and the spin-orbit coupling: $\mathbf{L}\cdot\mathbf{S} = -lsw_0^{110}$. Note that the relation for O^{xyz} does not hold for the magnetic dipole operator $T_z = \frac{l}{2l+3} w_0^{211}$ due to its definition in real instead of angular momentum space.

By summing Eqn. (19) over both spin-orbit split edges,

$$\overline{I}_0^z(j^+) + \overline{I}_0^z(j^-) = \frac{\langle w_0^{z0z}\rangle}{\langle n_h\rangle} \tag{21}$$

we obtain the sum rule that relates the total integrated intensity to the spin-independent operators.[15] ($\overline{I}$ indicates that the spectra are normalized to the isotropic spectrum). For $z = 1$ we have the "L_z" sum rule. In general, it relates the integrated intensity of $I_0^z(\omega)$ to spin-independent operators that give the 2^z-polar moment in the electron distribution. For $z = 0$ it simply says that the integrated intensity over both edges is proportional to the number of holes. For higher values of z the ground state expectation values of w^{z0z} show an oscillatory behaviour along the rare earth series, see Fig. 5. This behaviour is already well described by assuming a Hund's rule ground state.[28]

A weighted substraction of both edges can be related to the spin-dependent operators,

$$\overline{I}_0^z(j^+) - \frac{c+1}{c}\overline{I}_0^z(j^-) = \frac{1}{\langle n_h\rangle}\left\{\frac{z}{[z]}\langle w_0^{z-1,1,z}\rangle + \frac{z+1}{[z]}\langle w_0^{z+1,1,z}\rangle\right\} \tag{22}$$

For $z = 0$ this expression forms the basis of the theory of branching ratios.[26] It relates the integrated intensities of the spin-orbit split edges of the isotropic spectrum to the ground state expectation value of the spin-orbit operator (note that $w^{-1,1,0} = 0$). For $z = 1$ it gives the "S_z-T_z" sum rule.[16]

The assumption in deriving this equation is that a certain spin-orbit split edge can be described by the core hole having the corresponding j-value. This approximation is valid for late rare earths (and also late transition metals). For early rare earths deviations are found for the spin-dependent sum rule, see Fig. 5. Although for these systems a smaller spin-orbit coupling is found, this is not the dominant effect that causes the stronger mixing of the two edges. More important are the LSJ values that are reached by the absorption. For late rare earths the ground state has maximum LSJ values. As a result of the dipole selection rules ($\Delta S = 0, \Delta L = 0, \pm 1$) also high LSJ values for XAS final states are found. These states are predominantly found in the j^+-edge. A qualitative argument for this goes as follows. Within LS-coupling (i.e., no spin-orbit coupling) the $\underline{c}l^{n+1}$ states with high LS values have relatively low energies (where $\underline{c}$ indicates a core hole). After switching on the spin-orbit coupling the LS states with low energy predominantly go into the j^+-edge and those with high energy into the j^--edge. Hence, for the states with high LSJ values there is only small mixing between the two edges. The most extreme examples are the states with maximum LSJ values that only occur in the j^+-edge. The limited presence of high LSJ character in the j^- edge directly explains why the the L_2 and M_4 edge have little intensity for late rare earths.

The situation is different for early rare earths. First, the total J of the ground state is given by $|L - S|$. Second, for early rare earths the maximum spin of the XAS final states is higher than that of the ground state ($S_n^{\max} = S_g^{\max} + 1$).[26] Since in XAS $\Delta S = 0$ these states have little weight (as a result of the mixing by the spin-orbit coupling they obtain a finite intensity). For early rare earths excitations therefore occur at intermediate LSJ values. This can also be seen in the M_{45} XAS spectra where for early rare earths significant intensity only occurs at 5-10 eV above the absorption edge (which consists of the "dipole-forbidden" maximum spin states), see Fig. 3. The stronger mixing between the edges is directly apparent from strong intensity at both edges. This mixing has as a result that for early rare earths deviations for the spin-dependent sum rule are found, although for $z = 1$ the trends are well predicted.

B. $2p \to 5d$ XAS and elastic scattering

We now discuss the behaviour of XAS and resonant elastic scattering at the $2p \to 5d$ absorption edge. For elastic scattering, it is more convenient to couple the matrix elements of the excitation to those of the deexcitation instead of coupling the excitation and deexcitation to their complex conjugates, as was done for inelastic scattering, see Eqn. (11). One then obtains for dipolar transitions

$$I(\mathbf{k}\boldsymbol{\epsilon}\omega, \mathbf{k}'\boldsymbol{\epsilon}'\omega) = \frac{2\pi}{\hbar} N_\omega^2 \Big| \sum_{z,n} \frac{B_1^2}{\mathcal{E}_n} \mathbf{T}^z(\boldsymbol{\epsilon}, \boldsymbol{\epsilon}') \cdot \mathbf{I}^z(gnng) \Big|^2$$

where the angular dependence $\mathbf{T}^z(\boldsymbol{\epsilon}, \boldsymbol{\epsilon}')$ is given by Eqn. (14) under the replacement of $\boldsymbol{\epsilon}^*$ by $\boldsymbol{\epsilon}'^*$. For XAS, the $z = 1$ spectrum is selected by taking the difference between left and right circularly polarized light. In elastic scattering one adopts a $\sigma \to \pi$ scattering geometry, where σ and π denote linear polarization perpendicular to and in the scattering plane, respectively. From the expressions for $U^{11z}(\boldsymbol{\epsilon}_\sigma, \boldsymbol{\epsilon}_\pi, \hat{\mathbf{Z}})$, see Table II, one sees that the $z = 1$ contribution is obtained if $\hat{\mathbf{Z}}$, i.e., the magnetic axis, is in the scattering plane. Thus the $\sigma \to \pi$ spectrum can be approximately considered as the square of the circular dichroic XAS spectrum.

The difficulty in the interpretation of the $2p \to 5d$ circular dichroism is that the radial matrix elements are strongly affected by the presence of $4f$ electrons.[7] Since the radial extent of the $5d$ orbital depends on the direction of the $5d$ moment with respect to that of the $4f$ (and therefore on energy) deviations from the XAS sum rules should be found. This was indeed observed experimentally where the sign of the signal could not be reconciled with the expected direction of the magnetic moment.[31–33] The change in radial matrix element was first considered by band structure calculations.[7] However, in LDA the circular dichroic branching ratio is always -1, since only the $5d$-$4f$ spin interactions are considered. Recently, a model has been developed that includes the complete df-Coulomb interaction, i.e., also the orbital contributions.[14] The assumption was that the dichroic signal was mainly determined by the change in the radial matrix elements and that the $5d$ polarization in the ground has a relatively small effect, i.e., one can assume a $5d^0$ ground state. For constant radial matrix elements, the integrated intensity of the circular dichroism is then zero.[15,16] However, this does not mean a zero signal. As a result of the interaction with the $4f$ electrons the circular dichroic spectrum contains equal positive and negative parts. Note, that this implies a finite elastic scattering amplitude even in the absence of a $5d$ polarization in the ground state. Due to the large $2p$ lifetime broadening the spectrum for q-polarized light is mainly determined by its first moment, $\langle g|V_q^\dagger H_{df} V_q|g\rangle$.

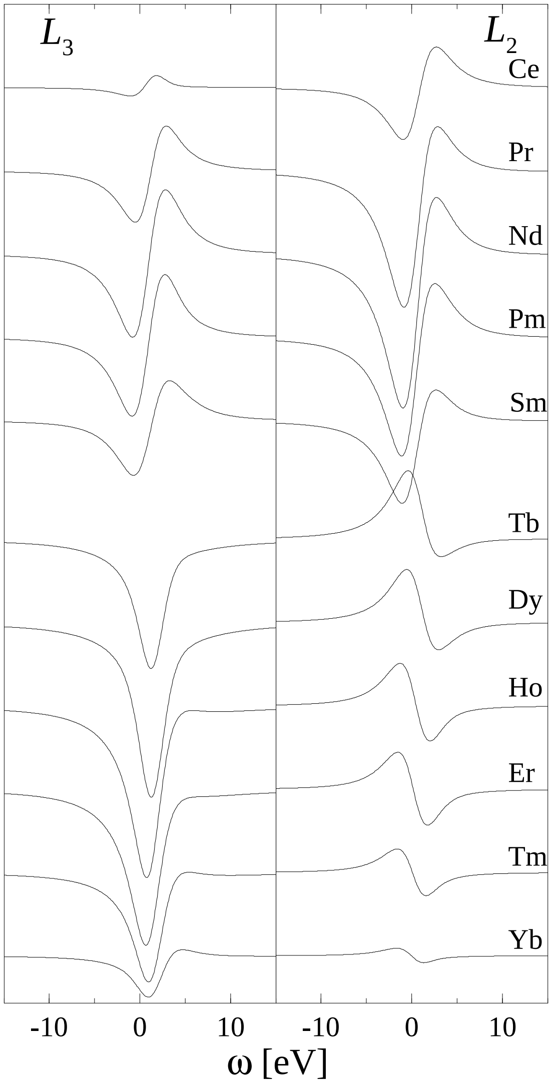

FIG. 6. Dipolar circular dichroic $2p \to 5d$ XAS spectra as a function of excitation energy ω for trivalent rare-earth ions. The left and right panel show the L_3 and L_2 edge, respectively. All spectra have the same scale.

Within a framework with fixed atomic orbitals one can create a $5d$ orbital with a different radial extent by mixing it with other nd orbitals, i.e., $|5\tilde{d}\rangle = a|5d\rangle + \sum_{n\neq 5} a_n |nd\rangle$. Using first order perturbation theory one finds[14] that the zeroth moment $\tilde{I}_0^z$ of the absorption spectrum into $5\tilde{d}$ is proportional to the first moment $I_0^{(1)z}$ of the absorption spectrum into $5d$:

$$\begin{aligned}\tilde{I}_0^z &= -\sum_{n\neq 5} \frac{2}{\Delta_{nd}} I_0^{(1)z}(n,j) \\ &= -\sum_{n\neq 5} \frac{2P_{5d}P_{nd}}{[cl]\Delta_{nd}} \sum_k G^k_{5d,4f;4f,nd} \\ &\qquad \times \sum_{xy} L_{kx}(df) M_y(j) N_{xyz} \langle w_0^{xyz} \rangle, \qquad (23)\end{aligned}$$

where Δ_{nd} is the energy difference between the $5d$ and a nd orbital, and

$$L_{kx}(df) = (-)^{x+k} n_{dkf}^2 \frac{[f]}{[c]} \frac{n_{fx}}{n_{dx}} \left\{ \begin{array}{ccc} f & f & k \\ d & d & x \end{array} \right\}. \tag{24}$$

The F^k direct Coulomb terms have been omitted since they do not contribute to the circular dichroic first moment. Note that the ground-state expectation values in Eqn. (23) are those of the $4f$ and not the $5d$ shell. The result looks very similar to the XAS sum rules of Eqn. (19). In particular, for the k=1 terms one has $L_{kx}(df) = 1/35$ and, except for a scaling, the same coefficients as for XAS are found.

Figure 6 shows numerical calculations of the $2p \rightarrow 5d$ circular dichroism at the L_{23} edges using final state configuration interaction between $\underline{2p}4f^{n+1}5d^1$ and $\underline{2p}4f^{n+1}nd^1$. To reduce the size of the calculations only the $6d$ orbital is included. To account for the other nd orbitals the Coulomb interactions between the $5d$ and the $6d$ shell are multiplied by four. The energy difference between the $5d$ and $6d$ orbitals has been taken 15 eV; only the $5d$ region is shown in the figure. The broadening is 6 eV which accounts for band effects and lifetime broadening. As a result of computer limitations we were unable to obtain results for Gd^{3+}. One would expect the spectrum to be given by a single negative peak at the L_3 edge and a positive peak with equal intensity at the L_2 edge.

Despite the crudeness of the model one finds qualitative agreement between theory and experiment.[31–33] For late rare earths the signal at the L_3 edge is larger than that at the L_2 edge, whereas for early rare earths the L_2 is the larger. The sign of the I_0^1 quadrupolar contribution to the absorption spectrum is opposite to that of the dipolar, except for the L_2 edge for $4f^9$ to $4f^{13}$ where the same sign is found. This difference is an effect of the G^3 and G^5 terms in Eqn (23). Also the relative signs of the edges are well predicted. For early rare earths both edges have the same sign, whereas for late rare earths an opposite sign is found.

One also observes that, for early rare earths and for the L_2 edges in late rare earths, the spectrum is more derivative-like than for the L_3 edge in late rare earths. This effect is also seen experimentally.[31,32] We do not have a satisfactory qualitative explanation for this effect. We also note that for the L_2 edge the signal occurs at lower energies with respect to the lowest final state. This effect, combined with the larger lifetime broadening of the L_2-edge, might explain why the quadrupole contributions are not always easily observed in the L_2 edge.

For finite $5d$ polarizations one can approximate the total intensity by $I_0^z + \tilde{I}_0^z$, where I_0^z is given by Eqn. (19). Note that the I_0^z and $\tilde{I}_0^z$ are given by $5d$ and $4f$ ground-state expectation values, respectively. Experiment shows that $\tilde{I}_0^z$ dominates. The trends in $|I_0^z|$ are similar to those of $|\tilde{I}_0^z|$, but their signs are usually opposite.[13] A finite $5d$ polarization therefore decreases the integrated intensity (in principle it could even change sign),[34] but has relatively little effect on the branching ratio.

C. Resonant inelastic x-ray scattering

For x-ray inelastic scattering sum rules one has to integrate over the incoming and outgoing photon energies. Let us first consider the integration over the transferred energy, $\Delta\omega = \omega - \omega'$, which leads to a term describing the decay of an intermediate state, $I_{\zeta'}^{z'}(n'n) = \sum_f I_{\zeta'}^{z'}(n'ffn)$. Note the presence of cross terms as a result of interference between intermediate states leading to the same final state. For the decay one has to distinguish two situations.

First, the core hole is filled by an electron from a shallower core level, leading to a Raman process described by $l^n \rightarrow \underline{c}l^{n+1} \rightarrow \underline{c}'l^{n+1}$. If both the intermediate and final states are split by the spin-orbit coupling the spectrum has four clearly separated manifolds. For a given manifold we find[28]

$$I_{\zeta'}^{z'}(nn';jj') = \mathcal{B}_{jj'}^{z'}(c,Q,c') \sum_{mm'} (-)^{j-m'} \begin{pmatrix} j & z' & j \\ -m' & \zeta' & m \end{pmatrix} \times \langle n'|c_{jm'} c_{jm}^{\dagger}|n\rangle n_{jz'}^{-1} , \tag{25}$$

with the coefficient given by

$$\mathcal{B}_{jj'}^{z'}(c,Q,c') = (-)^{j+j'+c+c'} P_{cc'}^2 [jj'] \left\{ \begin{array}{ccc} j & j' & Q' \\ c' & c & s \end{array} \right\}^2 \times \left\{ \begin{array}{ccc} Q' & Q' & j' \\ j & j & z' \end{array} \right\} n_{jz'} n_{Q'z'}^{-1} . \tag{26}$$

The decay of an intermediate state ($n = n'$) is therefore determined by an expectation value of the polarization of the core hole for that state. For, e.g., $z' = 1$ this expectation value is $\langle j_z \rangle$.

Let us consider a specific example. A typical resonant Raman process[9,10] is given by l=$4f$, c=$2p$, and c'=$3d$. For simplicity we take the incoming light isotropic. If the system is magnetic the absorption process still creates a polarized core hole as a result of the polarization of the valence shell. If the polarization is not detected the outgoing light has an isotropic and linear dichroic part, see Eqn. (16),

$$\frac{1}{2}\{I(\omega, \hat{\mathbf{k}}'\boldsymbol{\epsilon}^{+}\omega') + I(\omega, \hat{\mathbf{k}}'\boldsymbol{\epsilon}^{-}\omega')\} = \frac{2\pi}{\hbar} N_{\omega'} N_{\omega} B_1^2 B_2^2 \{I_0^{000}(\omega,\omega') + \frac{1}{2} C_0^2(\hat{\mathbf{k}}) I_0^{022}(\omega,\omega')\}.$$

Figure 7 gives the two different spectra for Ho^{3+} at three different incoming photon energies. If we now take, for a certain absorption energy, the difference of two spectra at different detection angles with respect to the magnetic axis, we obtain a signal that is proportional to $I_0^{022}(\omega,\omega')$. In that case the integration over ω' of a spectrum at a given absorption energy is finite at the L_3-edge, but zero at the L_2-edge, see Fig. 7. This is a direct result of the fact that the $j = \frac{1}{2}$ level has no quadrupolar moment (a finite intensity can still occur as a result of the presence

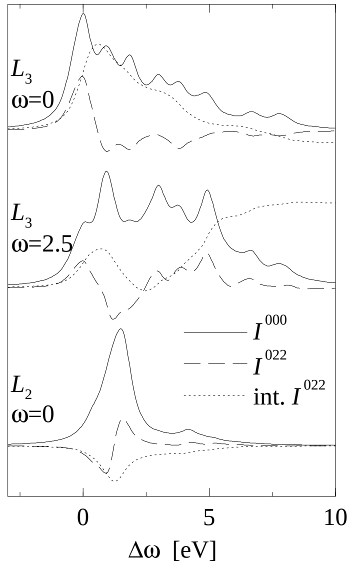

FIG. 7. RIXS spectra ($4f^n \to \underline{2p}4f^{n+1} \to \underline{3d}4f^{n+1}$) as a function of transferred energy $\Delta\omega = \omega - \omega'$. The zero of the energy scale corresponds to the energy of the lowest final state of a certain edge. Spectra are given at three excitation energies, from top to bottom: at the L_3 absorption edge, 2.5 eV above the L_3 absorption edge, at the L_2 absorption edge, see Fig. 1. Only the M_5 edge is shown. The incoming light is isotropic; the outgoing light is isotropic ($I_0^{000}(\omega,\omega')$, solid line) and linear dichroic ($I_0^{022}(\omega,\omega')$, dashed line). The dotted line gives the intensity of $I_0^{022}(\omega,\omega')$ integrated along the $\Delta\omega$ axis.

of $j = \frac{3}{2}$ character in the L_2 edge due to the mixing by the core-valence Coulomb interactions).

For a measurement with isotropic outgoing light the expectation value is proportional to $\delta_{n,n'}$, i.e., the decay is constant and all interference terms cancel. When a summation over both j'-edges is made one obtains[18,28]

$$I_0^{z'=0}(nn') = \sum_{j'} I_0^0(nn';jj') = \frac{P_{cc'}^2}{[c]}\delta_{n,n'} \ . \qquad (27)$$

Therefore, for isotropic outgoing light an integration over the transferred energy $\omega - \omega'$ leads to a spectrum as a function of excitation energy ω which is proportional to XAS.[18,28]

The second case is where the deexcitation involves the valence shell, i.e., $l^n \to \underline{c}l^{n+1} \to l^n$. Figures 3 and 4 show the spectra integrated over the energy of the outgoing photons (fluorescence yield) for isotropic and circular dichroic incoming light, respectively; the outgoing light has been taken isotropic. We observe significant differences with the XAS spectra. Therefore, even for isotropic outgoing light, the decay cannot be decoupled from the excitation. In contrast to Eqn. (25), where the operators working on the closed shell could be removed, one obtains here that the decay is proportional to an intermediate-state expectation value of a two-particle operator. For isotropic outgoing light one has[19]

$$\begin{aligned} I_0^{z'=0}(nn') = \frac{P_{cl}^2}{[c]}\{\delta_{n,n'} + \frac{1}{[l]n_{l1c}^2} \sum_{\lambda\lambda'\gamma\gamma'\sigma\sigma'} \delta_{\lambda'-\gamma',\lambda-\gamma} \\ \times\, c^1(c\gamma',l\lambda')c^1(c\gamma,l\lambda)\langle n'|l_{\lambda\sigma}c_{\gamma'\sigma'}l_{\lambda'\sigma'}^{\dagger}c_{\gamma\sigma}^{\dagger}|n\rangle\}, \end{aligned}$$

where $c^1(c\gamma,l\lambda)$ are the Slater-Condon parameters.[35] The matrix elements are, except for an offset and the radial integrals, equivalent to those of the G_{cl}^1 Coulomb exchange. Note that the "G_{cl}^1" term also assumes negative values and that the lowest possible value for $I_0^{z'=0}$ is zero. The G_{cl}^1 Coulomb term is also for a large part responsible for the position of the eigenstates in a spin-orbit manifold. This directly explains the trend in the fluorescence spectra, that the states closer to the absorption threshold in a certain edge have in general a smaller decay compared to those at the high-energy side of an edge.

Let us now consider the sum rules for the intensities integrated along the transferred and excitation energy. For deep-lying core levels with a large lifetime broadening, such as the $2p$ shell, one can use the fast-collision approximation.[17,18] This implies replacing the intermediate state energy denominator by $\overline{\mathcal{E}}_n = \omega + E_g - \overline{E}_n + i\frac{\Gamma}{2}$, where $\overline{E}_n$ is an average energy. For the situation where the emission involves two core levels one can then derive[18,28]

$$\begin{aligned} I_0^{zz'r}(j,j') &= \int_j d\omega \int_{j'} d\omega'\ I_0^{zz'r}(\omega,\omega') \\ &= \mathcal{B}_{jj'}^{z'}(c,Q,c')\sum_{xy}\mathcal{C}_j^{xyrzz'}(c,Q,l)\langle w_0^{xyr}\rangle \qquad (28) \end{aligned}$$

where the coefficients $\mathcal{B}$ and $\mathcal{C}$ are given in Ref. 28. For isotropic outgoing light we have $\mathcal{C}_j^{xyzz0} = \frac{P_{cl}^2}{[cl]}M_y(j)N_{xyz}$, which means that the same coefficients are found as for XAS. In this limit the fast-collision approximation is not necessary since all interference effects cancel.

When the deexcitation involves the valence states the situation is more complex. Sum rules would involve two-particle valence shell expectation values which are difficult to evaluate. Recently, an investigation has been made into the applicability of XAS sum rules for spectra obtained with fluorescence yield.[19] Although fluorescence yield is in principle not equal to XAS the conditions for integrated intensities are less stringent. Here one does not require that every final state has a constant decay but that the total decay of the excited intermediate states does not have a strong polarization dependence.

The state after excitation with q-polarized light can be written as $|v_q\rangle = \sum_n a_n(q)|n\rangle$; this state can be normalized to unity by using the coefficients $\overline{a}_n(q) = a_n(q)/\sqrt{\langle v_q|v_q\rangle}$. The integrated intensity of the fluorescence spectrum excited with q-polarized light can then be written as[19]

$$I_q^{\text{fluor}} = \langle v_q|v_q\rangle\langle V^\Gamma\rangle_q = I_q^{\text{XAS}}\langle V^\Gamma\rangle_q, \qquad (29)$$

i.e, the integrated intensity is given by the XAS intensity multiplied by a term that describes the radiative decay.

If the polarization of the outgoing light is not measured this latter term is given by

$$\langle V^{\Gamma}\rangle_q = \sum_{z' \text{ even}} \mathcal{T}_{z'} C_0^{z'}(\hat{\mathbf{k}}') \sum_{nn'} \frac{\pi}{\Gamma} \frac{\overline{a}_n \overline{a}_{n'}}{\left(\frac{E_n - E_{n'}}{\Gamma}\right)^2 + 1} I_0^{z'}(nn') \ .$$

This clearly shows that the total decay for q-polarized light $\langle V^{\Gamma}\rangle_q$ is a weighted average of the decays of the intermediate states $I_0^{z'}(nn')$. Proportionality of the integrated intensity of the circular dichroic fluorescence spectra, i.e., $(\sum_q q I_q^{\text{fluor}})/(\sum_q I_q^{\text{fluor}})$, with $\langle w^{101}\rangle = \langle L_z\rangle/l$ is obtained if $\langle V^{\Gamma}\rangle_q$ is not strongly dependent on the polarization. Numerical evaluation of $\langle V^{\Gamma}\rangle_q$ shows that this situation is found for early rare earths, but that there is a strong polarization dependence for late rare earths.[19] This can be understood as follows. As was shown above, the decay of the intermediate states is proportional to a "G^1_{cl}"-like term. Maximum variations in decay can be expected for "pure" LS-like intermediate states. The effect of mixing by the spin-orbit coupling is small for the high LSJ states that are reached in absorption in late rare earths, leading to a strong polarization dependence. The stronger mixing of the intermediate LSJ-states that are reached in early rare earths decreases variations in $\langle V^{\Gamma}\rangle_q$. It is remarkable that the mechanism that causes deviations for the "S_z" XAS sum rule improves the agreement between L_z values obtained by fluorescence yield and the ground-state expectation values.

It must be noted that a more efficient way to remove variations in $\langle V^{\Gamma}\rangle_q$ is to create a $|v_q\rangle$ which has not a strong LS-like character. This is found for many transition-metal systems where a strong crystal field quenches the orbital moment.

V. CONCLUSION

In conclusion, a comparison has been made between XAS and resonant inelastic x-ray scattering. Several aspects deserve further experimental investigation. The isotropic L_{23} spectra should be reexamined since, as was shown by Loeffen *et al.*,[11] more detailed information can be obtained by partial deconvolution of the lifetime broadening. This should enable a direct comparison of the relative size of the dipolar and quadrupolar contributions. Also a careful determination of the intensities of the two spin-orbit split edges would be interesting. It is generally assumed that for isotropic light $I^0_{L_3}/I^0_{L_2}=$ 2:1. However, a strong polarization of the $5d$ electrons in the ground state would give deviations from the statistical branching ratio. The $2p \rightarrow 5d$ circular dichroism certainly requires more experimental and theoretical research. Explanation of circular dichoism by band structure calculations have so far only considered the *df* spin interaction. The difficulties in explaining the circular dichroic branching ratios directly implies that the coupling of the $5d$ band to the local $4f$ states is not well understood. Band structure calculations including orbital polarization are necessary in the interpretation of the circular dichroism.

The experimental developments in x-ray inelastic scattering are more recent. It is now rather well established that on-resonance the excitation and decay cannot be decoupled. For a delocalized system this implies that one has to take into account the crystal momentum of the core hole (although core-valence interactions in the intermediate state might change its value). For a localized system one has to consider the angular momentum. Within an independent electron model the angular momentum is conserved. However, interactions with the valence shell change the values of j and m and in general for an intermediate-state eigenstate one has to consider expectation values of, e.g., j_z of the core hole. This quantity could be obtained by, e.g., measuring the difference between left and right circular polarization of the outgoing light. Unfortunately these experiments are rather complex. A determination of the quadrupolar moment of the core hole polarization seems more promising since it involves a measurement at two different detection angles. The presence of core-hole polarization has been demonstrated in resonant photoemission[36] ($l^n \rightarrow \underline{c} l^{n+1} \rightarrow \underline{c}'^2 l^{n+1} E_k$, where E_k denotes a photoelectron) which is formally very similar to the scattering process $l^n \rightarrow \underline{c} l^{n+1} \rightarrow \underline{c}' l^{n+1}$. Recent resonant Raman experiments on Co show the presence of higher moments in the core hole distribution.[37]

The x-ray scattering process $l^n \rightarrow \underline{c} l^{n+1} \rightarrow l^n$ enables one to study valence band excitations. Although for electric multipole transitions $\Delta S = 0$, these excitations also include spin flips, since the spin is not a good quantum number in the intermediate state as a result of the large core-hole spin-orbit coupling. Recently, octet-sextet transitions have been observed in Gd^{3+} (ground state $^8S_{\frac{7}{2}}$).[38]

A relatively simple way to study resonant inelastic x-ray scattering is fluorescence yield, since it does not involve the detection of the energy of the outgoing photon. The spectra for fluorescence yield already show significant deviations from the XAS cross section.

APPENDIX A:

The tensor products in this paper are done with $3j$-symbols which are up to a factor equivalent to those with Clebsch-Gordan coefficients

$$\begin{aligned}[][\mathbf{a}^l, \mathbf{b}^{l'}]^x_\xi &= \sum_{\lambda\lambda'} a^l_\lambda b^{l'}_{-\lambda'} (-1)^{l-\lambda-\lambda'} \begin{pmatrix} l & x & l' \\ -\lambda & \xi & \lambda' \end{pmatrix} \\ &= (-1)^{l'} [x]^{-\frac{1}{2}} \sum_{\lambda\lambda'} a^l_\lambda b^{l'}_{\lambda'} C^{x\xi}_{l\lambda,l'\lambda'} \ . \qquad \text{(A1)}\end{aligned}$$

When more than one superscript is present the last one gives the rank of the tensor; a tensor without superscript has rank one. Furthermore, we often make use of the numerical factors

$$n_{lx} = \begin{pmatrix} l & x & l \\ -l & 0 & l \end{pmatrix} = \frac{(2l)!}{\sqrt{(2l-x)!(2l+1+x)!}} \tag{A2}$$

and

$$n_{xyz} = \begin{pmatrix} x & y & z \\ 0 & 0 & 0 \end{pmatrix}. \tag{A3}$$

The latter factor is zero for odd $x+y+z$. In certain cases it is convenient to have a "generalized" form for n_{xyz}:

$$\begin{aligned} \underline{n}_{xyz} = {} & i^g \left(\frac{(g-2x)!(g-2y)!(g-2z)!}{(g+1)!} \right)^{\frac{1}{2}} \\ & \times \frac{g!!}{(g-2x)!!(g-2y)!!(g-2z)!!} \end{aligned} \tag{A4}$$

with $g = x+y+z$. Note that n_{xyz} is equal to $\underline{n}_{xyz}$ for even g. The purpose of these factors is to remove the square roots from the expressions. These square roots are a result of the normalization of the $3j$-symbols which is inconvenient when dealing with physical quantities, such as, operators and combinations of spectra.

Some useful tensor products are: the inner product, $[\mathbf{a}^l,\mathbf{b}^l]^0_0 n_{l0}^{-1} = \mathbf{a}^l \cdot \mathbf{b}^l$, the outer product, $[\mathbf{a},\mathbf{b}]^1 = -\frac{i}{\sqrt{6}} \mathbf{a} \times \mathbf{b}$, and the coupling of two spherical harmonics of the same vector $[\mathbf{C}^l(\hat{\mathbf{k}}),\mathbf{C}^{l'}(\hat{\mathbf{k}})]^x = \mathbf{C}^x(\hat{\mathbf{k}})(-)^l n_{ll'x}$. In this paper we also apply the orthogonality relation $(\mathbf{a}^l \cdot \mathbf{b}^l)(\mathbf{c}^{l'} \cdot \mathbf{d}^{l'}) = \sum_x [x][\mathbf{a}^l,\mathbf{c}^{l'}]^x \cdot [\mathbf{b}^l,\mathbf{d}^{l'}]^x$ with $[x] = 2x+1$.

---

[1] G. Schütz, W. Wagner, W. Wilhelm, P. Kienle, R. Frahm, and G. Materlik, Phys. Rev. Lett. **58**, 737 (1987).

[2] G. van der Laan, B. T. Thole, G. A. Sawatzky, J. B. Goedkoop, J. C. Fuggle, J.-M. Esteva, R. C. Karnatak, J. P. Remeika, and H. A. Dabkowska, Phys. Rev. B **34**, 6529 (1986).

[3] D. Gibbs, D. R. Harshman, E. D. Isaacs, D. B. McWhan, D. Mills, and C. Vettier, Phys. Rev. Let. **61**, 1241 (1988).

[4] J. P. Hannon, G. T. Trammell, M. Blume, and D. Gibbs, Phys. Rev. Lett. **61**, 1245 (1988).

[5] P. Carra and M. Altarelli, Phys. Rev. Lett. **64**, 1286 (1990).

[6] P. Carra, B. N. Harmon, B. T. Thole, M. Altarelli, and G. A. Sawatzky, Phys. Rev. Lett. **66**, 2495 (1991).

[7] X. D. Wang, T. C. Leung, B. N. Harmon, and P. Carra, Phys. Rev. B **47**, 9087 (1993); J. C. Lang, S. W. Kycia, X. D. Wang, B. N. Harmon, A. I. Goldman, D. J. Branagan, R. W. McCallum, K. D. Finkelstein, *ibid.* **46**, 5298 (1992).

[8] P. Fischer, G. Schütz, S. Stähler, and G. Wiesinger, J. Appl. Phys **69**, 6144 (1991); K. Shimomi, H. Maruyama, K. Kobayashy, A. Koizumi, H. Yamazaki, and T. Iwazumi, Jpn. J. Appl. Phys. **32-2**, 314 (1992); J. C. Lang, G. Srajer, C. Detlefs, A. I. Goldman, H. König, X. Wang, B. N. Harmon, and R. W. McCallum Phys. Rev. Lett. **74**, 4935 (1995).

[9] K. Hämäläinen, D. P. Siddons, J. B. Hastings, and L. E. Berman, Phys. Rev. Lett. **67**, 2850 (1991).

[10] M. H. Krisch, C. C. Kao, F. Sette, W. A. Caliebe, K. Hämäläinen, and J. B. Hastings, Phys. Rev. Lett. **74**, 4931 (1995).

[11] P. W. Loeffen, R. F. Pettifer, S. Müllender, M. van Veenendaal, J. Röhler, and D. S. Sivia, Phys. Rev. B **54**, 14 877 (1996).

[12] B. N. Harmon and A. J. Freeman, Phys. Rev. B **10**, 1979 (1974).

[13] T. Jo and S. Imada, J. Phys. Soc. Jpn. **62**, 3721 (1993).

[14] M. van Veenendaal, J. B. Goedkoop, and B. T. Thole, Phys. Rev. Lett. **78**, 1162 (1997).

[15] B. T. Thole, P. Carra, F. Sette, and G. van der Laan, Phys. Rev. Lett. **68**, 1943 (1992).

[16] P. Carra, B. T. Thole, M. Altarelli, and X. Wang, Phys. Rev. Lett. **70**, 694 (1993).

[17] J. Luo, G. T. Trammell, and J. P. Hannon, Phys. Rev. Lett. **71**, 287 (1993).

[18] P. Carra, M. Fabrizio, and B. T. Thole, Phys. Rev. Lett. **74**, 3700 (1995).

[19] M. van Veenendaal, J. B. Goedkoop, and B. T. Thole, Phys. Rev. Lett. **77**, 1508 (1996).

[20] D. A. Varshalovich, A. N. Moskalev, and V. K. Khersonskii, *Quantum Theory of Angular Momentum* (World Scientific, Singapore, 1988).

[21] B. T. Thole and G. van der Laan, Phys. Rev. B **49**, 9613 (1994).

[22] R. D. Cowan *The Theory of Atomic Structure and Spectra* (University of California Press, Berkeley, 1981).

[23] B. T. Thole, G. van der Laan, J. C. Fuggle, G. A. Sawatzky, R. C. Karnatak, J.-M. Esteva, Phys. Rev. B **32**, 5107 (1985).

[24] J. B. Goedkoop, B. T. Thole, G. van der Laan, G. A. Sawatzky, F. M. F. de Groot, and J. C. Fuggle, Phys. Rev. B **37**, 2086 (1988).

[25] S. Imada and T. Jo, J. Phys. Soc. Jpn. **59**, 3358 (1990).

[26] B. T. Thole and G. van der Laan, Phys. Rev. A **38**, 1943 (1988); Phys. Rev B **38**, 3158 (1988).

[27] B. T. Thole, G. van der Laan, and M. Fabrizio, Phys. Rev. B **50**, 11 466 (1994).

[28] M. van Veenendaal, P. Carra, and B. T. Thole, Phys. Rev. B **54**, 16 010 (1996); Note that here of the reduced matrix elements P_{cl} only $[cl]^{\frac{1}{2}}$ is maintained.

[29] B. R. Judd, *Second Quantisation in Atomic Spectroscopy* (Johns Hopkins University Press, Baltimore, 1967).

[30] P. Carra, H. König, B. T. Thole, and M. Altarelli, Physica B **192**, 182 (1993).

[31] F. Baudelet, Ch. Giorgetti, S. Pizzini, Ch. Brouder, E. Dartyge, A. Fontaine, J. P. Kappler, and G. Krill, J. El. Spec. **62** (1993) 153.

[32] Ch. Giorgetti, Ph. D. Thesis, University of Paris-Sud (unpublished).

[33] C. Giorgetti *et al.*, Phys. Rev. B **48** (1993) 12 732.

[34] H. Matsuyama, I. Harada, and A. Kotani, accepted for publication in the J. Phys. Soc. Jpn.

[35] E. U. Condon and G. H. Shortley, *The Theory of Atomic Spectra* (Cambridge University Press, Cambridge, 1951).

[36] B. T. Thole, H. A. Dürr, and G. van der Laan, Phys. Rev. Lett. **74**, 2371 (1995).

[37] L. Braicovich *et al.*, (unpublished).

[38] C. Dallera, L. Braicovich, C. Ghiringhelli, M. van Veenendaal, J. B. Goedkoop, and N. B. Brookes, accepted for publication in Phys. Rev. B.